Comparisons of Global Topographic/Isostatic Models To the Earth's Observed Gravity Field

by
Reiner Rummel
Delft University of Technology
Richard H. Rapp
The Ohio State University
Department of Geodetic Science and Surveying
Hans Sünkel
Technical University Graz
and
C. Christian Tscherning
Geodetic Institute of Denmark

Report No. 388

Department of Geodetic Science and Surveying
The Ohio State University
Columbus, Ohio 43210-1247

March 1988

COMPARISONS OF GLOBAL TOPOGRAPHIC/ISOSTATIC MODELS TO THE EARTH'S OBSERVED GRAVITY FIELD

by

Reiner Rummel

Delft University of Technology

Richard H. Rapp

The Ohio State University

Hans Sünkel

Technical University Graz

C. Christian Tscherning

Geodetic Institute of Denmark

Report No. 388

Department of Geodetic Science and Surveying

The Ohio State University

Columbus, Ohio 43210-1247

March 1988

Abstract

The earth's gravitational potential, as described by a spherical harmonic expansion to degree 180, has been compared to the potential implied by the topography and its isostatic compensation using five different hypothesis. Initially, series expressions for the Airy/Heiskanen topographic/isostatic model were developed to the third order in terms of (h/R) where h is equivalent rock topography and R is a mean earth radius. Using actual topographic developments for the earth, we found the second and third terms of the expansion contributed (on average) 30% and 3%, respectively, of the first term, of the expansion. With these new equations it is possible to compute depths (D) of compensation, by degree, using three different criteria: I) the power in the actual field at a specified degree should be the same as implied by the Airy/Heiskanen model; II) the topographic isostatic reduced potential should show minimum correlation with the earth's topography; III) the norm of the residual potential should be a minimum. The results show that the average (over all degrees) depth implied by criterion I is 60 km while it is about 33 km for criteria II and III with smaller compensation depths at the higher degrees. Another model examined was related to the Vening-Meinesz regional hypothesis implemented in the spectral domain. The fifth model tested took D to be a constant of 30 km at all degrees. We have compared these model fields with the actual field in terms of anomaly, geoid undulation and percentage differences, as well as with correlation coefficients and anomaly maps in the Caribbean/South America region. The differences between all models is small with the exception of the model defined by criterion I is used where larger differences are seen. For example, the average percentage differences between the OSU81 potential model and the five models outlined above, from degrees 15 through 180 is 87.2(I), 80.5(II), 79.8(III), 80.1(VM), 80.5(D=30km). Finally oceanic and continental response functions are derived from the global data sets and comparisons made to locally determined values.

Foreword

This report was prepared by Reiner Rummel, of the Delft University of Technology (Afdeling der Geodesie), Richard H. Rapp, The Ohio State University (Department of Geodetic Science and Surveying), Hans Sünkel, Technical University Graz (Institute of Mathematical Geodesy), and C. Christian Tscherning, Danish Geodetic Institute. The effort of one of the authors (RHR) was supported through NASA Grant NGR 36-008-161, The Ohio State University Research Foundation Project No. 783210. This grant is administered through the NASA Goddard Space Flight Center.

Computer support at Ohio State was provided by the Instruction and Research Computer Center.

This report is a revision of a version originally submitted for publication. Comments made by reviewers of the original version were used in preparing this report.

The reproduction and distribution of this report was carried out with funds supplied, in part, by the Department of Geodetic Science and Surveying.

Table of Contents

1. Introduction

In recent years very efficient computer algorithms have been developed for spherical harmonic analysis up to high degrees and orders, (Colombo, 1981). In addition, terrestrial gravity material has become much more complete, through the results of satellite altimetry, see e.g. (Rapp, 1981). These facts and the availability of a global set of 1°x1° mean elevations make it very attractive to re-evaluate the older studies on global isostasy, carried out by Balmino et al. (1973) and others. A first step in this direction was an article by Rapp (1982). In Figure 1 of his paper a number of potential degree variance spectra are displayed. The spectrum of the "observed" gravity and the one derived from topographic heights and based on the Airy compensation model with a compensation depth of 50 km agree almost perfectly for the degrees 50 to 180. One may imply the following ideas from this figure:

1. A compensation depth D=50 km seems to be much more realistic than the generally accepted one of D=30 km for the Airy model.
2. Since the two spectra agree for n>50 but deviate for n<50 it may be feasible to apply an isostatic reduction to the observed gravity and, isolate those parts in the anomalous gravity field, that are not compensated isostatically, but are due to lateral inhomogenities in the earth's mantle.

It is of general interest in geodesy, whether or not the potential of the isostatically compensated topography could be used as a device for the smoothing of the earth's gravity field, before it is used in geodetic approximation techniques, similar to the practice in local gravity field approximation (Forsberg and Tscherning, 1981). We realize that the full study of isostasy is a complicated issue. Isostatic behavior can vary from region to region and can be dependent on numerous factors that we do not consider. Nevertheless we feel that it is important to find out what we can learn from the models we formulate.

2. Basic Equations for Airy Isostatic Model

The gravitational potential at a point P outside the earth Σ is by Newton's law of gravitation

$$V(P) = G \int_{\Sigma} \frac{\rho(Q)}{\ell_{PQ}} \, d\Sigma_Q \qquad (1)$$

with G, the gravitational constant, ρ the density inside the earth, ℓ the distance between P and the infinitesimal volume element $d\Sigma_Q$ at Q. We insert for the inverse distance $1/\ell_{PQ}$ its spherical harmonic expansion:

$$\frac{1}{\ell_{PQ}} = \frac{1}{r_P} \sum_{n=0}^{\infty} \left(\frac{r_Q}{r_P}\right)^n \frac{1}{2n+1} \sum_{m=0}^{n} \bar{P}_{nm}(\cos\theta_P) \, \bar{P}_{nm}(\cos\theta_Q) \, [\cos m\lambda_P \cos m\lambda_Q + \sin m\lambda_P \sin m\lambda_Q] \qquad (2)$$

where $\bar{P}_{nm}$ is the fully normalized associated Legendre function.
In a shorter notation:

$$\frac{1}{\ell_{PQ}} = \frac{1}{r_P} \sum_{n,m,\alpha} \left(\frac{r_Q}{r_P}\right)^n \frac{1}{2n+1} Y_{nm\alpha}(P)\, Y_{nm\alpha}(Q)$$

with

$$Y_{nm\alpha}(P) = \bar{P}(\cos\theta_P) \begin{cases} \cos m\lambda_P & \text{for } \alpha=0 \\ \sin m\lambda_P & \text{for } \alpha=1 \end{cases} \tag{3}$$

If we further assume that the geocentric radius r_P of P is greater than the radius of convergence of the series in (3), then (1) becomes after rearrangement

$$V(P) = \sum_{n,m,\alpha} r_P^{-(n+1)} \left\{\frac{G}{2n+1} \int_\Sigma r_Q^n\, \rho(Q)\, Y_{nm\alpha}(Q)\, d\Sigma_Q\right\} Y_{nm\alpha}(P)$$

$$= \frac{GM}{R} \sum_{n,m,\alpha} \left(\frac{R}{r_P}\right)^{n+1} \left\{\frac{1}{M(2n+1)} \int_\Sigma \left(\frac{r_Q}{R}\right)^n \rho(Q)\, Y_{nm\alpha}(Q)\, d\Sigma_Q\right\} Y_{nm\alpha}(P) \tag{4}$$

with M, the mass of the earth and R its mean radius. From equation (4) follows the well-known expression

$$V(P) = \frac{GM}{R} \sum_{n,m,\alpha} \left(\frac{R}{r_P}\right)^{n+1} C_{nm\alpha}\, Y_{nm\alpha}(P) \tag{5}$$

with the dimensionless coefficients

$$\left.\begin{matrix} \bar{C}_{nm} \\ \bar{S}_{nm} \end{matrix}\right\} = C_{nm\alpha} = \frac{3}{\bar{\rho}R^3(2n+1)} \frac{1}{4\pi} \int_\Sigma \left(\frac{r_Q}{R}\right)^n \rho(Q)\, Y_{nm\alpha}(Q)\, d\Sigma_Q \tag{6}$$

where M is replaced by $4/3\pi\bar{\rho}R^3$ and $\bar{\rho}$ is the mean density of the earth.

We consider now the model of <u>local isostatic compensation by Airy</u>. The coefficients of the potential generated by isostatically compensated topography $C^I_{nm\alpha}$ become, with equation (6):

$$C^I_{nm\alpha} = \frac{3}{R\bar{\rho}(2n+1)} \frac{1}{4\pi} \int_\sigma [A^T(Q) - A^C(Q)]\, Y_{nm\alpha}(Q)\, d\sigma_Q \tag{7}$$

The integration is performed over the unit sphere σ. The <u>surface topography part</u> is

$$A^T(Q) = \int_{r=R}^{R+h} \left(\frac{r_Q}{R}\right)^{n+2} \rho_{cr}(Q)\, dr_Q \tag{8}$$

with h, the surface elevation, and ρ_{cr} the density of the topography in land areas. In ocean areas ρ_{cr} is replaced by $\rho_{cr}-\rho_w$, where ρ_w is the density of sea water. The compensation part in equation (7) is:

$$A^C(Q) = \int_{r=R-D-t}^{R-D} \left(\frac{r_Q}{R}\right)^{n+2} \Delta\rho(Q)\, dr_Q \tag{9}$$

with D, the depth of compensation, t, the root (or anti-root) thickness,

$\Delta\rho=\rho_m-\rho_{cr}$, and ρ_m the density of the mantle. If it is assumed that neither ρ_{cr}, or $\rho_{cr}-\rho_w$, respectively, nor $\Delta\rho$ vary in radial direction, integration yields:

$$A^T(Q) = \rho_{cr}(Q)\,\frac{R}{n+3}\left[\left(\frac{R+h(Q)}{R}\right)^{n+3} - 1\right] \tag{10}$$

and

$$A^C(Q) = \Delta\rho(Q)\,\frac{R}{n+3}\left[\left(\frac{R-D}{R}\right)^{n+3} - \left(\frac{R-D-t(Q)}{R}\right)^{n+3}\right] \tag{11}$$

In practical computations h(Q) is replaced by mean elevations usually 1°x1°. For the geographical distribution of the densities one could in principle employ a classification into land, lake, sea, and ice areas. In practice, considering the limited quality of the data material, we can only distinguish between land and ocean areas with

$$\rho_j = \begin{cases} \rho_{cr} = 2670\ \frac{kg}{m^3} & \text{for } h_j>0 \quad \text{(land)} \\ \rho_{cr}-\rho_w = (2670-1030)\ \frac{kg}{m^3} & \text{for } h_j<0 \quad \text{(oceans)} \end{cases} \tag{12}$$

The derivation of the root thickness t shall be dealt with in the next chapter.

With A^T and A^C evaluated e.g. in blocks of 1°x1° and inserted into equation (7), the coefficients $C^I_{nm\alpha}$ of the isostatically compensated topography can be computed. Based on 5°x5° mean elevations such a computation was carried out by Lachapelle (1976) up to degree and order 36.

3. Condition of Equilibrium

The root thickness t(Q) is derived from the Airy model of local isostatic compensation. The equilibrium of mass condition between an element of mass at the surface and that at depth becomes for a spherical earth:

$$\int_{r=R}^{R+h} \rho_{cr}\, r^2\, dr\, d\sigma = \int_{r=R-D-t}^{R-D} \Delta\rho r^2\, dr\, d\sigma$$

or

$$\frac{\rho_{cr}}{3}\left[(R+h)^3 - R^3\right] = \frac{\Delta\rho}{3}\left[(R-D)^3 - (R-D-t)^3\right]. \tag{13}$$

We rewrite it as a third-order equation in $\frac{t}{R-D}$:

$$\left(\frac{t}{R-D}\right)^3 - 3\left(\frac{t}{R-D}\right)^2 + 3\left(\frac{t}{R-D}\right) - \frac{\rho_{cr}}{\Delta\rho}\left(\frac{R}{R-D}\right)^3\left[\left(\frac{h}{R}\right)^3 + 3\left(\frac{h}{R}\right)^2 + 3\left(\frac{h}{R}\right)\right] = 0$$

or simply as:

$$T^3 - 3T^2 + 3T - \eta[H^3 + 3H^2 + 3H] = 0 \tag{14}$$

with $T = \frac{t}{R-D}$, $H = \frac{h}{R}$, and $\eta = \frac{\rho_{cr}}{\Delta\rho}\left(\frac{R}{R-D}\right)^3$. An iterative solution with the starting value $T_o = \eta H$ yields up to the third order:

$$T = T_o + \Delta T = \eta H[1 + H(\eta+1) - \frac{1}{3} H^2 (\eta^3-1)] \tag{15}$$

or

$$t = \frac{\rho_{cr}}{\Delta\rho} \left(\frac{R}{R-D}\right)^2 h \left[1 + \frac{h}{R} (\eta+1) - \frac{1}{3} \left(\frac{h}{R}\right)^2 (\eta^2-1)\right] \tag{16}$$

Since $h/R < 2 \cdot 10^{-3}$ and $\eta \approx 4.5$ the error of a linear approximation remains below 1%. Hence we shall compute the root-thickness from

$$t = \frac{\rho_{cr}}{\Delta\rho} \left(\frac{R}{R-D}\right)^2 h = 4.45 \left(\frac{R}{R-D}\right)^2 h \tag{17}$$

with $\Delta\rho = \rho_m - \rho_{cr} = 3270 \frac{kg}{m^3} - 2670 \frac{kg}{m^3}$.

4. Series Expansion of Topographic and Isostatic Effects

The problem with the direct application of formulas (10) and (11) for the computation of A^T and A^C, is, that they have to be computed anew at each block for each degree n. Hence, even with very efficient computer algorithms a high degree and order expansion, say n(max) = 100 or 200 becomes very tedious and time consuming. An alternative approach starts from a binomial expansion of the expressions in brackets of equations (10) and (11). Up to third order in h/R it is:

$$A^T(Q) = \rho_{cr}(Q) \frac{R}{n+3} \left[1 + (n+3) \frac{h(Q)}{R} + \frac{(n+3)(n+2)}{2} \left[\frac{h(Q)}{R}\right]^2 + \frac{(n+3)(n+2)(n+1)}{6} \left[\frac{h(Q)}{R}\right]^3 + (0^4) - 1\right] \approx$$

$$\approx \rho_{cr}(Q)\, h(Q) \left[1 + \frac{n+2}{2} \frac{h(Q)}{R} + \frac{(n+2)(n+1)}{6} \left[\frac{h(Q)}{R}\right]^2\right] \tag{18}$$

A corresponding expansion of equation (11) yields

$$A^C(Q) = \Delta\rho(Q) \frac{R}{n+3} \left[\left[\frac{R-D}{R}\right]^{n+3} - \left[\frac{R-D}{R}\right]^{n+3} \left[1 - (n+3) \frac{t(Q)}{R-D} + \frac{(n+3)(n+2)}{2} \left[\frac{t(Q)}{R-D}\right]^2 - \frac{(n+3)(n+2)(n+1)}{6} \left[\frac{t(Q)}{R-D}\right]^3 + (0^4)\right]\right] \approx$$

$$\approx \Delta\rho(Q)\, t(Q) \left[\frac{R-D}{R}\right]^{n+2} \left[1 - \frac{n+2}{2} \frac{t(Q)}{R-D} + \frac{(n+2)(n+1)}{6} \left[\frac{t(Q)}{R-D}\right]^2\right] \tag{19}$$

The question is now at what term the series expansion has to be truncated without committing an unacceptably large error.

We assume as an upper bound for h=10 km and take for R=6370 km, D=30 km, and $t \approx (\rho_{cr}/\Delta\rho)h \approx 4.45 \cdot h = 44.5$ km. The resulting values of the first, second, and third order terms in the brackets of equations (18) and (19) are listed in Table 1 for a number of degrees n. Because of the chosen high value of h the numbers in Table 1 have the character of upper bounds. Still,

Table 1: Contribution of the second and third order terms in equations (18) and (19) relative to the first order term.

	A^T Terms		A^C Terms	
n	$\frac{n+2}{2}\frac{h}{R}$	$\frac{(n+2)(n+1)}{6}\frac{h^2}{R^2}$	$\frac{n+2}{2}\frac{t}{R-D}$	$\frac{(n+2)(n+1)}{6}\frac{t^2}{(R-D)^2}$
2	0.003	0.0	0.014	0.0
10	0.009	0.0	0.042	0.001
50	0.041	0.001	0.186	0.023
100	0.080	0.004	0.364	0.088
200	0.158	0.017	0.721	0.345

in order to keep the truncation error below 10%, the second order terms have to be included for degrees greater than about 150 when computing A^T, and for degrees greater than about 30, when computing A^C. For A^C one should even consider the inclusion of the third order for degrees higher than 150. The numbers in Table 1 are not very sensitive to changes in D. In conclusion for the high degree and order expansions, considered in this study the inclusion of at least the second order is required, in contrast to what is stated in (Dorman & Lewis, 1970, p. 3359).

However, there is an additional aspect. We are actually interested in the combined effect of A^T and A^C, namely A^T-A^C, which enters into equation (7). If we insert for the root-thickness t from equation (17)

$$t(Q) = \frac{\rho_{cr}}{\Delta\rho}\frac{R^2}{(R-D)^2}\,h(Q)$$

we find

$$A^T(Q) - A^C(Q) = \rho_{cr}h\left\{\left[1-\left(\frac{R-D}{R}\right)^n\right] + \frac{n+2}{2}\left[1+\frac{\rho_{cr}}{\Delta\rho}\left(\frac{R-D}{R}\right)^{n-3}\right]\frac{h}{R}\right.$$
$$\left. + \frac{(n+2)(n+1)}{6}\left[1-\frac{\rho_{cr}^2}{\Delta\rho^2}\left(\frac{R-D}{R}\right)^{n-6}\right]\left(\frac{h}{R}\right)^2\right\} \qquad (20)$$

The alternating sign of the series expansion of A^C causes the first order term to almost cancel and since $\left(\frac{R-D}{R}\right)^n$ converges very slowly, it is true even for high degrees of n. The percentage values of the second, and third order terms in equation (20) relative to the first order are displayed in Figure 1. We see that throughout the entire spectrum from degree 2 to 200, the upper bound value (h=10 km) for the second order term either exceeds or remains little less than the first order term. The third order term reaches 25% of the first and second order for high degrees. If the upper bound value h=10 km is replaced by the approximate root mean square value of the topography of

about 2.5 km, the order of magnitude still remains between 18 and 46% of the first order, whereas the third order drops to below 1% in this case.

Now we insert equation (20) into equation (7), where ocean depths d_j (which are negative in magnitude) are replaced by equivalent rock topography, (see (12)):

$$h_j = \frac{\rho_{cr}-\rho_w}{\rho_{cr}} d_j = 0.614\ d_j \qquad \text{for } h_j < 0 \tag{21}$$

Then the (fully normalized) coefficients (up to and including 3rd order) are:

$$\begin{aligned} C^I_{nm\alpha} = \frac{3}{2n+1}\frac{\rho_{cr}}{\bar{\rho}} \Bigg\{ \left[1 - \left(\frac{R-D}{R}\right)^n\right] \frac{1}{4\pi}\int_Q \frac{h(Q)}{R} Y_{nm\alpha}(Q)\, d\sigma_Q + \\ + \frac{n+2}{2}\left[1 + \frac{\rho_{cr}}{\Delta\rho}\left(\frac{R-D}{R}\right)^{n-3}\right] \frac{1}{4\pi}\int \frac{h^2(Q)}{R^2} Y_{nm\alpha}(Q)\, d\sigma_Q \\ + \frac{(n+2)(n+1)}{6}\left[1 - \frac{\rho_{cr}^2}{\Delta\rho^2}\left(\frac{R-D}{R}\right)^{n-6}\right] \frac{1}{4\pi}\int \frac{h^3(Q)}{R^3} Y_{nm\alpha}(Q)\, d\sigma_Q \Bigg\} \end{aligned} \tag{22}$$

With the surface spherical harmonic expansions

$$h_{nm\alpha} = \frac{1}{4\pi}\int_\sigma \frac{h(Q)}{R} Y_{nm\alpha}(Q)\, d\sigma_Q,$$

$$h2_{nm\alpha} = \frac{1}{4\pi}\int_\sigma \frac{h^2(Q)}{R^2} Y_{nm\alpha}(Q)\, d\sigma, \text{ and} \tag{23,a-c}$$

$$h3_{nm\alpha} = \frac{1}{4\pi}\int_\sigma \frac{h^3(Q)}{R^3} Y_{nm\alpha}(Q)\, d\sigma\ ,$$

we obtain

$$\begin{aligned} C^I_{nm\alpha} = \frac{3}{2n+1}\frac{\rho_{cr}}{\bar{\rho}} \Bigg\{ \left[1 - \left(\frac{R-D}{R}\right)^n\right] h_{nm\alpha} + \frac{n+2}{2}\left[1 + \frac{\rho_{cr}}{\Delta\rho}\left(\frac{R-D}{R}\right)^{n-3}\right] h2_{nm\alpha} \\ + \frac{(n+2)(n+1)}{6}\left[1 - \frac{\rho_{cr}^2}{\Delta\rho^2}\left(\frac{R-D}{R}\right)^{n-6}\right] h3_{nm\alpha}\Bigg\}\ . \end{aligned} \tag{24}$$

This is the series expansion up to 3rd order for the computation of the potential coefficients of the isostatically reduced topography. In practice very often only the very convenient formulas of the first order expansion are used. They can be interpreted as a double layer expansion. But as we saw, this may result in considerable distortions in the computed coefficients. The need for a second order expansion was already emphasized in (Jung, 1950) with calculations carried out by Uotila (1965). In Arnold (1980) the second order expansion has been treated, too. The evaluation of the series expansion represented by (24) is much more efficient than the evaluation of the rigorous equations given by Lachapelle (1976). A comparison of coefficients computed from the rigorous application of (10) and (11) to the series results represented by (24) shows agreement on the order of $0.2\text{x}10^{-9}$.

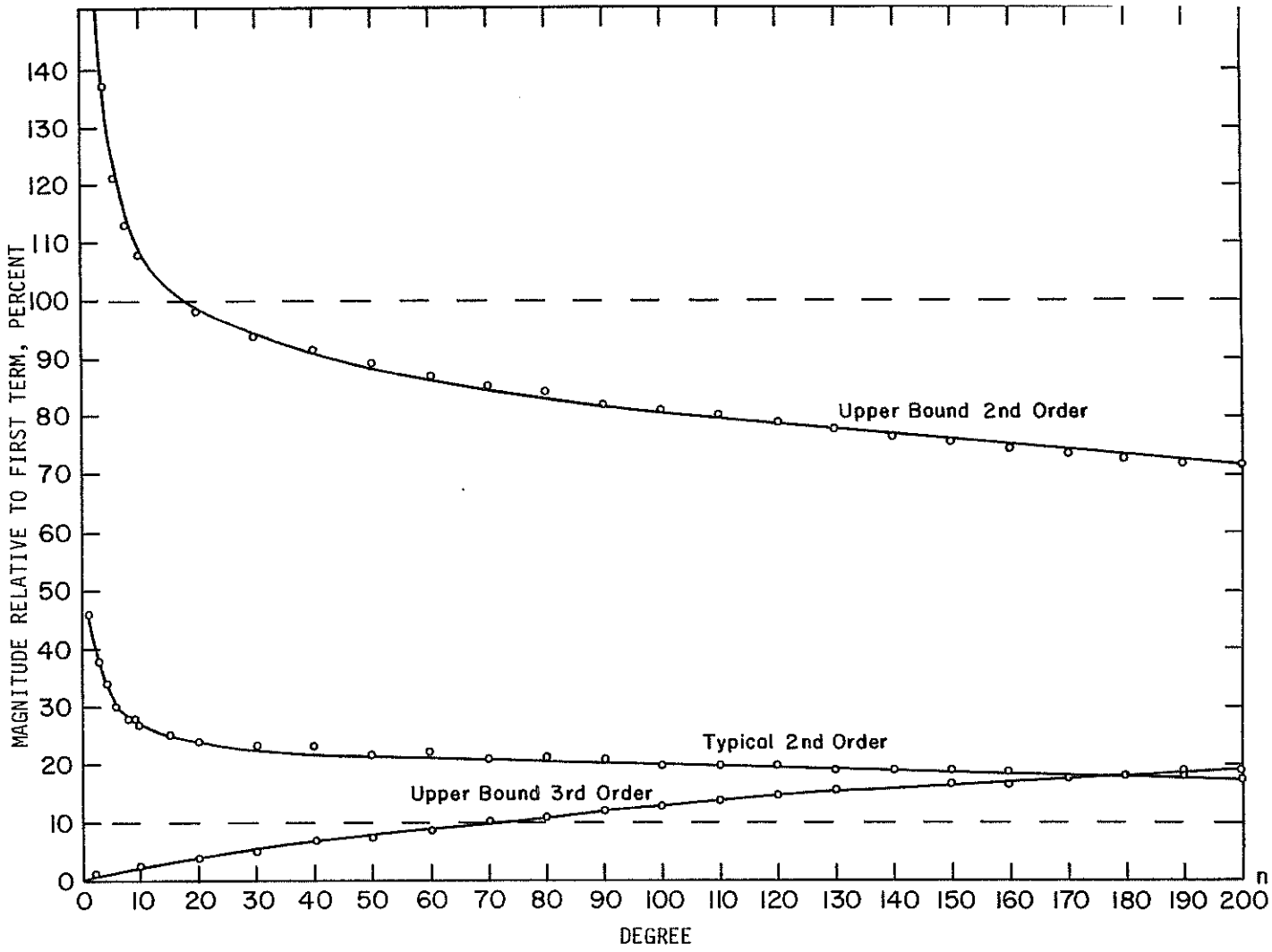

Figure 1. Percent Values of Second and Third Terms of A^T-A^C Equation (20) Relative to the First Term as a Function of Degree.

In numerical tests we noted that the power spectra of $(h/R)^2$ and $(h/R)^3$ were approximately 10^{-6} and 10^{-13}, respectively, of the power of (h/R). However to see the whole picture we examined the relative contributions of the $h_{nm\alpha}$, $h2_{nm\alpha}$, and $h3_{nm\alpha}$ terms to the topographic-isostatic potential at various degrees. We found that the $h2_{nm\alpha}$ contribution is on average 30% (a maximum of 110%) of the $h_{nm\alpha}$ contribution while the $h3_{nm\alpha}$ terms contributes an average of 3% (maximum 11%) of the $h_{nm\alpha}$ contribution. These figures are consistent with the estimates made earlier. The significant role of the second terms is caused by the small value of the coefficient of $h_{nm\alpha}$ in (27).

Another computation was the comparison of the potential implied by the three, two and one term topographic/isostatic models with D=30km. The anomaly, undulation, and percentage difference by degree were calculated. (See Section 8 for equations). The overal difference (degrees 2 to 180) between the three and one term models was 1.5m, 4.4mgal, and 35%. These differences were essentially the same (1.5m, 4.4mgal, 34%) for the two vs one term model. The magnitude of the undulation difference was greatest at the lower degrees while the anomaly and percentage differences were similar independent of degree. It is clear from these comparisons that a substantial error is caused by using only the first term in the model. For subsequent calculations, we will use the two term model.

We finally note here that the series expression for the potential coefficients of the uncompensated topography can be written from (24) by letting D=R. We have:

$$C^T_{nm\alpha} = \frac{3}{2n+1}\frac{\rho_{cr}}{\bar{\rho}}\left\{ h_{nm\alpha} + \frac{n+2}{2} h2_{nm\alpha} + \frac{(n+2)(n+1)}{6} h3_{nm\alpha} \right\} \qquad (25a)$$

The coefficients of the isostatic compensation would be:

$$C^C_{nm\alpha} = \frac{3}{2n+1}\frac{\rho_{cr}}{\bar{\rho}}\left\{\left(\frac{R-D}{R}\right)^n h_{nm\alpha} - \frac{n+2}{2}\frac{\rho_{cr}}{\Delta\rho}\left(\frac{R-D}{R}\right)^{n-3} h2_{nm\alpha} + \frac{(n+2)(n+1)}{6}\frac{\rho^2_{cr}}{\Delta\rho^2}\left(\frac{R-D}{R}\right)^{n-6} h3_{nm\alpha}\right\} \qquad (25b)$$

The coefficients of the isostatically compensated topography would then be:

$$C^I_{nm\alpha} = C^T_{nm\alpha} - C^C_{nm\alpha} \qquad (25c)$$

with equation (24) representing this difference.

5. Preliminary Comparisons

For the first series of numerical results we have computed the potential coefficient spectrum implied by the topography, and by the isostatically compensated topography. The spectrum of a set of coefficients A would be:

$$\sigma_n^2(A) = \sum_m \sum_\alpha C^2_{nm\alpha} = \sum_m (\bar{C}^2_{nm} + \bar{S}^2_{nm}) \qquad (26)$$

The elevations and depths for these computations have been taken from a 1°x1° mean elevation file (TUG86.DTM) described by Sünkel (1986). This file is based on land elevations received from the Defense Mapping Agency Aerospace

Center in 1983 (with corrections for 12 values) and an averaging of a 5'x5' data set (NGDC, 1983) over the oceans. In ocean areas the depths (d) were converted to rock equivalent topography using the nominal density of the crust and sea water using equation (21). No special consideration was given to ice areas because of lack of information.

The harmonic coefficients of h/R and $(h/R)^2$ were computed to degree 180 using program HARMIN (Colombo, 1981) using integrated associated Legendre functions. These coefficients are represented by equation (23, a,b,c). With these coefficients the potential coefficients of the uncompensated topography ($C^I_{nm\alpha}$) and the isostatically compensated topography ($C^I_{nm\alpha}$) have been computed for the nominal compensation depth of D = 30 km. Plots of the spectra (from equation (26)) are shown in Figure 2. Also shown in this figure is the spectrum implied by the observed gravitational field of the earth as described by the OSU81 (Rapp, 1981) model which is complete to degree 180. From this figure we see the significant power in the uncompensated topography that is considerably reduced when isostatic compensation is taken into account. However the power of the D = 30 km case is less than that in the observed field which was noted by Rapp (1982).

In Section 8 we will consider a number of comparisons between the observed potential field and model fields. At this point, however, we must discuss how the appropriate value of D is selected.

6. Optimal Compensation Depths

The isostatically reduced gravity potential dV is obtained by subtracting the potential due to the isostatically compensated topography, V^I, from the "observed" gravity potential V:

$$dV(P) = V(P) - V^I(P) \tag{27}$$

If the isostatic hypothesis of Airy fit reality perfectly, dV would be free of all influences of the earth's crust and solely reflect the lateral density inhomogeneities of the earth's core and mantle. As mentioned in the introduction, from the degree variance spectra of V and of V^I for the compensation depths D=30 km and 50 km in Rapp (1982), one might conclude that a compensation depth of 50 km is more realistic than one of 30 km. However, if one derives, from (27), the formula connecting the degree variance spectra of dV, V, and V^I, we have:

$$\sigma_n^2(V) = \sigma_n^2(V^I) + 2\mathrm{cov}_n(V^I, dV) + \sigma_n^2(dV) \tag{28}$$

One sees, that an agreement of $\sigma_n^2(V)$ and $\sigma_n^2(V^I)$ does not necessarily imply that $\sigma_n^2(dV)$ is small. One also has to take into account the covariance $\mathrm{cov}(V^I, dV)$.

We shall now discuss the computation of optimal compensation depths per degree, still within the Airy type model of compensation. Thus, the compensation depth D shall become a function of degree n. Three models for different optimality criteria shall be discussed.

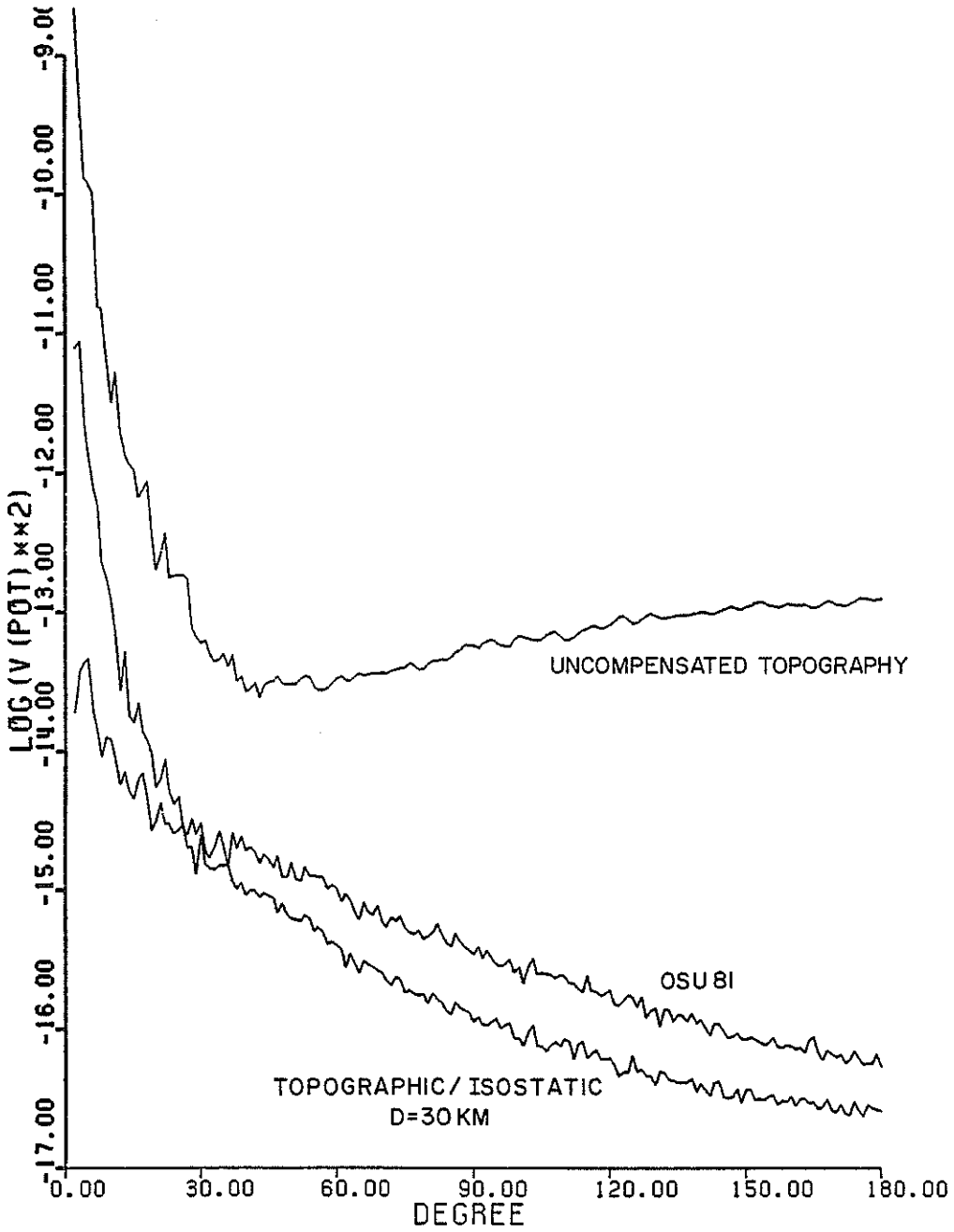

Figure 2. Log of the Potential Degree Variances of the OSU81 Potential Coefficient Solution; the Potential Implied by Uncompensated Topography, and the Potential Implied by Topographic/Isostatic Compensation with D=30 km, as a Function of Spherical Harmonic Degree.

Criterion 1: $\sigma_n^2(V) = \sigma_n^2(V^I)$

As mentioned above this criterion has little physical relevance. Its application shall only result in an optimal agreement of the degree variances of the observed gravity field, $\sigma_n^2(V)$, and of the topographic-isostatic model, $\sigma_n^2(V^I)$. It does not necessarily produce a small residual field of dV. The criterion is included only for the purpose of showing that its application leads to compensation depths D_n of about 50 km. To evaluate this definition we form the following function:

$$f(D_n) \equiv \sigma_n^2(V) - \sigma_n^2(V^I(D_n)) = 0 \tag{29}$$

with

$$\sigma_n^2(V) = \sum_m \sum_\alpha (C_{nm\alpha})^2 \tag{30}$$

and with equation (24)

$$\begin{aligned}\sigma_n^2(V^I(D_n)) &= \sum_m \sum_\alpha (C^I_{nm\alpha})^2 \\ &= \sum_m \sum_\alpha \left\{\frac{3}{2n+1}\frac{\rho_{cr}}{\bar\rho}\left\{\left[1 - \left(\frac{R-D_n}{R}\right)^n\right]h_{nm\alpha} + \frac{n+2}{2}\left[1 + \frac{\rho_{cr}}{\Delta\rho}\left(\frac{R-D_n}{R}\right)^{n-3}\right]h2_{nm\alpha}\right.\right. \\ &\quad \left.\left. + \frac{(n+2)(n+1)}{6}\left[1 - \frac{\rho_{cr}^2}{\Delta\rho^2}\left(\frac{R-D}{R}\right)^{n-6}\right]h3_{nm\alpha}\right\}\right\}^2 \\ &= \sum_m \sum_\alpha \left\{A_n[1 - Q_n^n]h_{nm\alpha} + B_n\left[1 + \frac{\rho_{cr}}{\Delta\rho}Q_n^{n-3}\right]h2_{nm\alpha} + \text{---}\right\}^2 \end{aligned} \tag{31}$$

with $A_n = \frac{3}{2n+1}\frac{\rho_{cr}}{\bar\rho}$, $B_n = A_n\frac{n+2}{2}$, and $Q_n = \frac{R-D_n}{R}$

For the computation of the approximate compensation depths D_n^o the linear model for $C^I_{nm\alpha}$ is employed:

$$C^I_{nm\alpha} \approx A_n[1 - Q_n^n]h_{nm\alpha} \tag{32}$$

From

$$\begin{aligned} f^o(D_n^o) &= \sigma_n^2(V) - A_n^2[1 - Q_n^n]^2 \sum_m \sum_\alpha h^2_{nm\alpha} \\ &= \sigma_n^2(V) - A_n^2[1 - Q_n^n]^2\sigma_n^2(h) = 0 \end{aligned} \tag{33}$$

which can be solved for D_n^o in the following steps:

$$\begin{aligned} 1 - Q_n^n &= \sqrt{\frac{\sigma_n^2(V)}{A_n^2\sigma_n^2(h)}} \\ 1 - \left(\frac{R-D_n^o}{R}\right)^n &= \frac{\sigma_n(V)}{A_n\sigma_n(h)} \\ D_n^o &= R\left[1 - \left(1 - \frac{\sigma_n(V)}{A_n\sigma_n(h)}\right)^{1/n}\right] \end{aligned} \tag{34}$$

Based upon the approximate values D_n^o, the actual depths can be obtained by

Newton iteration. We write:

$$D_n^{i+1} = D_n^i - \frac{f(D_n^i)}{f'(D_n^i)} \tag{35}$$

with the derivative f' of f from equations (30) and (31) and where the superscript i is an iteration index.

$$f'(D_n^i) = \frac{\partial f}{\partial D_n}\Big|_{D_n^i}$$

$$= 2 \sum_m \sum_\alpha C^I_{nm\alpha}(D_n^i)\left\{A_n \frac{n}{R}\left[\frac{R-D_n^i}{R}\right]^{n-1} h_{nm\alpha} - B_n \frac{\rho_{cr}}{\Delta\rho}\frac{n-3}{R}\left[\frac{R-D_n^i}{R}\right]^{n-4} + \text{---}\right\}$$

and $f' \neq 0$.

Using the OSU81 field and the rock equivalent topography expansions D_n values have been computed. They are listed in Table 2, column 2 and displayed in Figure 3. The average D value is 64 km for degrees 2 to 180, and 58 km for degrees 30 to 180.

Table 2. Depth (D) of Airy Compensation Based on Three Criteria

Degree	Criteria			
	1	2	3	Vening-Meinesz
5	144 km	0	0	29
10	94	65	64	29
15	54	40	40	29
20	40	27	27	30
25	40	31	31	30
30	34	22	23	30
50	52	30	31	31
70	49	29	30	31
90	60	30	30	32
110	61	35	37	32
130	79	38	40	33
150	56	29	32	34
170	68	25	29	34
175	61	31	33	35
180	56	26	29	35

Criterion 2: $|\mathrm{cov}_n(V^T, dV)| = \min$

A very valid requirement is the choice of the depths of compensation such that the topographic-isostatic reduced potential dV shows minimum correlation with the earth's topography. The correlation can be expressed as:

$$\mathrm{cov}_n(V^T, dV) = \sum_m \sum_\alpha C^I_{nm\alpha} dC_{nm\alpha} \tag{37}$$

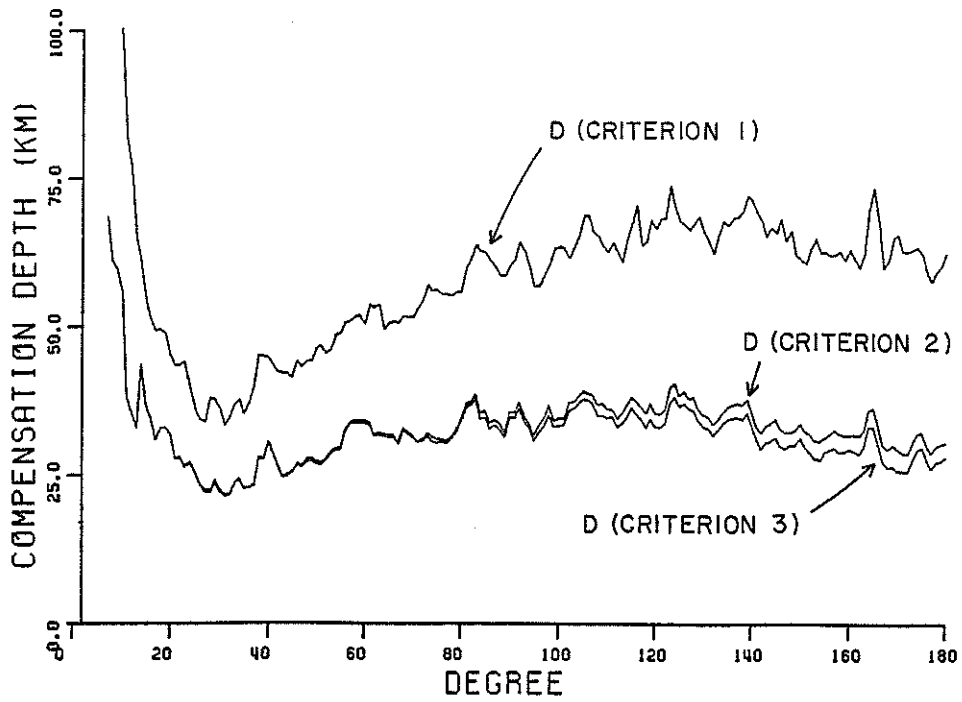

Figure 3. Compensation Depths for the Three Criteria Considered as a Function of Spherical Harmonic Degree.

or using equations (25c):

$$\mathrm{cov}_n(V^T,\ dV) = \sum_m \sum_\alpha C^T_{nm\alpha}(C_{nm\alpha} - C^T_{nm\alpha} + C^C_{nm\alpha})$$

$$= \mathrm{cov}_n(V,\ V^T) - \sigma_n^2(V^T) + \mathrm{cov}_n(V^T,\ V^C) \qquad (38)$$

In linear approximation equation (37) becomes with the definitions in (31):

$$\mathrm{cov}_n(V^T,\ dV(D_n^o)) = A_n\mathrm{cov}_n(V,\ h) - A_n^2\sigma_n^2(h) + A_n^2Q^n\sigma_n^2(h) \qquad (39)$$

If by definition $D_n^o = \{D_n^o |\ 0 \leq D_n^o \leq R\}$ then $A_n^2Q^n\sigma_n^2(h)$ is a monotonously decreasing function with

$$A_n^2Q^n\sigma_n^2(h) = \begin{cases} A_n^2\sigma_n^2(h) & \text{for } D_n^o = 0 \\ 0 & \text{for } D_n^o = R \end{cases} \qquad (40)$$

Now three cases can be distinguished in order to attain the minimum of $\mathrm{cov}_n(V^T,\ dV(D_n^o))$:

if $A_n\mathrm{cov}_n(V,\ h) - A_n^2\sigma_n^2(h) > 0 \Rightarrow D_n^o = R$

if $A_n\mathrm{cov}_n(V,\ h) - A_n^2\sigma_n^2(h) < A_n^2\sigma_n^2(h) \Rightarrow D_n^o = 0$

otherwise, $|\mathrm{cov}_n(V^T,\ dV(D_n^o))| = \min$ implies:

$$\mathrm{cov}_n(V^T,\ dV(D_n^o)) = 0$$

Then, with equation (39):

$$Q^n = \frac{A_n^2\sigma_n^2(h) - A_n \mathrm{cov}_n(V, h)}{A_n^2\sigma_n^2(h)} = 1 - \frac{\mathrm{cov}_n(V, h)}{A_n\sigma_n^2(h)}$$

or

$$D_n^o = R\left[1 - \left(1 - \frac{\mathrm{cov}_n(V, h)}{A_n\sigma_n^2(h)}\right)^{1/n}\right] \tag{41}$$

For the actual solution, again the three cases $D_n = R$, $D_n = 0$, and $0 < D_n < R$ can be distinguished. In the latter case, i.e. $0 < D_n < R$, the compensation depths are derived from a Newton iteration, as before, with $f(D_n) = \mathrm{cov}_n(V^T, dV)$ according to equation (38).

The resulting compensation depths are listed in Table 2, column 3, and displayed graphically in Figure 3. The average D value is 32 km for degrees 2 to 180, and 31 km for degrees 30 to 180.

Criterion 3: $\|dV\|^2 = \min$

Whereas criterion 2 seems to be more relevant for geophysicists, the next criterion (3) is especially interesting for geodetic application. In geodesy topographic-isostatic reduction is mainly applied to produce a smooth residual field which allows simple and accurate interpolation. This is achieved with criterion 3. It is:

$$\begin{aligned}\|dV\|^2 &= \sum_n \left\{\sum_m \sum_\alpha \left[C_{nm\alpha} - C^I_{nm\alpha} + C^c_{nm\alpha}(D_n)\right]^2\right\} \\ &= \sum_n \left\{\sum_m \sum_\alpha \left[C^2_{nm\alpha} + (C^I_{nm\alpha})^2 + (C^c_{nm\alpha}(D_n))^2 - 2C_{nm\alpha}C^I_{nm\alpha}\right.\right. \\ &\quad \left.\left. + 2C_{nm\alpha}C^c_{nm\alpha}(D_n) - 2C^I_{nm\alpha}C^c_{nm\alpha}(D_n)\right]\right\}. \end{aligned} \tag{42}$$

$\|dV\|^2 = \min.$ is obtained from a solution of

$$\sum_m \sum_\alpha \left(C^c_{nm\alpha}\frac{\partial C^c_{nm\alpha}}{\partial D_n} + C_{nm\alpha}\frac{\partial C^c_{nm\alpha}}{\partial D_n} - C^I_{nm\alpha}\frac{\partial C^c_{nm\alpha}}{\partial D_n}\right) = 0$$

or $$\sum_m \sum_\alpha \frac{\partial C^c_{nm\alpha}}{\partial D_n} dC_{nm\alpha} = 0 \tag{43}$$

In linear approximation, $\frac{\partial C^c_{nmax}}{\partial D_n}$, with equation (25b), can be written:

$$\begin{aligned}\frac{\partial C^c_{nm}}{\partial D_n} &= -A_n \frac{n}{R} Q^{n-1} h_{nm\alpha} \\ &= -\frac{n}{R} Q^{n-1} C^I_{nm\alpha}\end{aligned}$$

Consequently equation (43) becomes:

$$-\frac{n}{R} Q^{n-1}\mathrm{cov}_n(V^T, dV) = 0 \tag{44}$$

Equation (44) is satisfied either by

I: $Q^{n-1} = \left(\frac{R-D_n^o}{R}\right)^{n-1} = 0$

which is true for $D_n^o = R$, or by

II: $\mathrm{cov}_n(V^T, dV) = 0$

which is identical to the linear case of criterion 2, treated above. Solution I leads to $C_{nm\alpha}^c = 0$, and results in a pure Bouguer reduction, compare equation (25). In contrast to solution II, solution I represents a maximum of equation (42) and is therefore of no interest. Hence, in linear approximation, criteria 2 and 3 agree, or in other words the minimum norm of dV and minimum correlation of V^T and dV result in one and the same compensation depths D_n^o.

In second and higher order approximation, $\|dV\|^2 = \text{min.}$ differs from $|\mathrm{cov}(V^T, dV)| = \text{min.}$ The solution is again obtained by Newton iteration with equation (42) in the following form:

$$f(D_n) = \sum_m \sum_\alpha \frac{\partial C_{nm\alpha}^c}{\partial D_n} dC_{nm\alpha}$$

$$= \sum_m \sum_\alpha \left\{ - A_n \frac{n}{R} Q^{n-1} h_{nm\alpha} + B_n \frac{n-3}{R} \frac{\rho_{cr}}{\Delta\rho} Q^{n-4} h2_{nm\alpha} - \cdots \right\}$$
$$\left\{ C_{nm\alpha} - A_n(1-Q^n) h_{nm\alpha} - B_n \left[1 + \frac{\rho_{cr}}{\Delta\rho} Q^{n-3}\right] h2_{nm\alpha} + \cdots \right\}$$

$$f(D_n) = Q^{n-1} \left\{ - \frac{n}{R} A_n \left[\mathrm{cov}_n(V, h) - A_n(1-Q^n)\sigma_n^2(h) - B_n \right.\right.$$
$$\left[1 + \frac{\rho_{cr}}{\Delta\rho} Q^{n-3}\right] \mathrm{cov}_n(h, h^2) \left.\right] + \frac{n-3}{R} \frac{\rho_{cr}}{\Delta\rho} B_n Q^{-3}$$
$$\left.\left[\mathrm{cov}_n(V, h^2) - A_n(1-Q^n)\mathrm{cov}_n(h, h^2) - B_n \left[1 + \frac{\rho_{cr}}{\Delta\rho} Q^{n-3}\right] \sigma_n^2(h^2) \right] \right\} \qquad (45)$$

from which $f'(D_n) = \frac{\partial f}{\partial D_n}$ follows by straightforward differentiation.

The resulting compensation depths are given in Table 2, column 4 and displayed in Figure 3. They differ from those obtained from criterion 2 typically by 1 to 2 km with the greatest differences at the higher degrees. The average D value is 33 km for both degrees 2 to 180 and 30 to 180.

At this point we have three different procedures to compute the depth of compensation by degree. Given the depths, which will depend to some extent on a potential and topographic model of the earth, the topographic/isostatic potential can be computed using equation (24) with D now a function of n. Numerical comparisons between these and other models will be discussed in Section 8.

7. Optimal Vening Meinesz Isostatic Models

Half a century ago Vening Meinesz argued that the simple isostatic concept of Airy/Heiskanen, which is governed by a strictly local compensation, is not very realistic because, due to its elasticity, the mantle is able to support a

certain amount of local topographic load without local yielding, whereas in the Airy/Heiskanen model free mobility between vertical mass columns is presupposed - a highly unlikely assumption (Vening Meinesz, 1939). Therefore, he proposed a regional compensation model which is now denoted the Vening Meinesz model (Heiskanen and Moritz, 1967).

Regional mass compensation can be described by a smoothing operator, applied to the non-smoothed isostatic masses implied by the Airy/Heiskanen model. This idea has been pursued by Sünkel (1985, 1986). In the following we shall describe how to best estimate both the depth of compensation and the parameter(s) of the smoothing operator.

In linear approximation the harmonic coefficients of the topographic/isostatic potential for the Airy/Heiskanen model are given by

$$C^I_{nm} = \frac{3}{2n+1} \frac{\varrho_{cr}}{\bar{\rho}} \left[1 - \left[\frac{R-D}{R}\right]^n\right] h_{nm\alpha} \tag{46}$$

(cf. eq. (24)), where the term with "1" is the contribution of the topography, and the term with $((R-D)/R)^n$ is the contribution of its isostatic compensation.

If the isostatic masses are subject to a smoothing procedure, implied by a homogeneous and isotropic smoothing operator B,

$$B(P,Q) = \sum_{n=0}^{\infty} (2n+1)\, \beta_n\, P_n\, (\cos\psi_{PQ}) \tag{47a}$$

with eigenvalues β_n,

$$\beta_n = 2\pi \int_{-1}^{1} B(t)\, P_n\, (t)dt \tag{47b}$$

(P_n ... Legendre polynomial; $t := \cos\psi$; ψ ... spherical distance), we then obtain, by observing the convolution theorem, the harmonic coefficients of the topographic/isostatic potential in linear approximation for a Vening Meinesz model,

$$C^I_{nm} = \frac{3}{2n+1} \frac{\varrho_{cr}}{\bar{\rho}} \left[1 - \left[\frac{R-D}{R}\right]^n \beta_n\right] h_{nm\alpha} \,. \tag{48}$$

(Note that the topographic part remains unchanged; only the isostatic part changes because of smoothing!)

Various models for the set of eigenvalues $\{\beta_n\}$ could be envisioned, each particular model controlling the features of the corresponding smoothing operator β. We list here a very few:

a) $\beta_n = 1 \;\forall\; n$
In this particular case there is no smoothing involved. Therefore, this operator represents the standard Airy/Heiskanen model with the compensation depth D as the only parameter.

b) $\beta_0 = 1,\ \beta_n = 0 \;\forall\; n > 0$
In this case the smoothing operator degenerates into the global average operator with equal weight; the smoothed compensation masses form a

homogeneous layer which is equivalent to a point mass at the origin. Therefore, this operator represents the other extreme case of the Airy/Heiskanen model where the "level" of compensation is at the origin, D = R.

c) $\beta_n = 0 \; \forall \; n$
This set of eigenvalues represents the annihilation operator which annihilates all isostatic masses. Therefore, only topographic masses are left (unchanged) in this particular case. Consequently, the corresponding harmonic coefficients are those of the topography only, which represent the topographic potential.

d) With

$$\beta_n := \left[\frac{R-D_n}{R-D}\right]^n$$

a smoothing operator is implied which is identical to the isostatic model used in section 6: a model where the compensation depth formally depends on the degree n, rather than being constant as in the general case of eq. (48). We think it is important to stress and therefore, we repeat it: the multi-compensation depth model discussed in section 6 represents, in linear approximation, also some type of smoothing operator which is applied to the compensation masses.

It should be obvious that there exists an infinite number of other models for the eigenvalues $\{\beta_n\}$ of the smoothing operator B, e.g. $e^{-b^2n^2}$ or the like; (here b is the only model parameter of the smoothing operator). Generally, the smoothing operator of eq. (47a) depends on a certain number p of model parameters; together with the compensation depth parameter D we have therefore to estimate p+1 parameters of the isostatic model.

The three optimization criteria for the estimation of the model parameters, which have been discussed in section 6, can be applied here as well. In principle the estimation procedures agree with those of section 6 with two small differences:

a) In the case of the Vening Meinesz model each harmonic $C^I_{nm\alpha}$ depends on all p+1 model parameters, while in section 6 a harmonic of degree n depended exclusively on the degree-specific compensation depth D_n:
b) through the smoothing procedure, the operator B enters into higher degree terms like $h2_{nm\alpha}$, $h3_{nm\alpha}$, ... in a rather complicated manner, requiring for its computation a (quickly converging) iteration procedure.

Because of property (a) the estimation of the degree-specific compensation depths D_n according to criteria I - III of section 6 is possible on a degree by degree basis. Here, in the general smoothing model approach, this is no longer possible (exception: β_n according to model (d)). Instead of the solution of N_{max} (= highest degree of model) optimization problems with one parameter D_n, we have to solve now one optimization problem with p+1 parameters.

Because of property (b) an iteration procedure is involved: eq. (48) presupposes a linear relation between the harmonic coefficients of the topographic-isostatic potential and the topographic height. But according to eq. (25b) this relation is non-linear because of the higher degree terms $h2_{nm\alpha}$, $h3_{nm\alpha}$, ... (Note that in the Vening Meinesz model $h_{nm\alpha}$ is replaced by $\beta_n\ h_{nm\alpha}$; therefore $h^J{}_{nm\alpha}$ is the harmonic coefficient of the smoothed topography B*h, raised to the power J). Therefore, the following iteration process offers itself:

step 0: i = 0
get a priori estimates for the isostatic model parameters $\hat{D}^{(0)}$ and $\hat{b}^{(0)}$ (here b is the vector comprising all p parameters of the chosen smoothing operator); harmonic analysis of the topography and its low powers, yielding $h_{nm\alpha}$, $h2_{nm\alpha}$, ...;

step 1: i := i + 1
smoothing of compensation masses, implied by $B^{(i-1)}*h$ using $\hat{D}^{(i-1)}$ and $\hat{b}^{(i-1)}$, yielding a smoothed topography $h^{(i)}$;

step 2: harmonic analysis of low powers of $h^{(i)}$ yielding a first order term $C^{I}_{nm}{}^{(i)}$ of eq. (48) which will be considered as a function of D and b, and higher order (correction) terms $C2^{I}_{nm}{}^{(i)}$, $C3^{I}_{nm}{}^{(i)}$, ... which will be considered as constants in the subsequent step;

step 3: optimal estimation solution (least-squares adjustment or least-squares collocation with parameters) for D and b with Taylor point $\hat{D}^{(i-1)}$, $\hat{b}^{(i-1)}$ and linearization restricted to the linear term $C^{I}_{nm}{}^{(i)}$ of step 2; stop if $|\hat{D}^{(i)} - \hat{D}^{(i-1)}| < \varepsilon_D$ and $|\hat{b}^{(i)} - \hat{b}^{(i-1)}| < \varepsilon_b$, else go to (1).

The result of this iteration process yields both best estimates for the isostatic model parameters (compensation depth D and the parameters of the smoothing operator B), and the set of harmonic coefficients of the topograhic - isostatic potential of the implied Vening Meinesz model.

This procedure has been applied to the determination of a two parameter model with D = constant and $\beta_n = e^{-b^2n^2}$. The result is D=29 km and b=0.00223. The values of D_n found by setting $\beta_n = e^{-b^2n^2}$ to $((R-D_n)/(R-D))^n$ are shown in Table 2. The values are similar to the other values above degree 20.

8. Observed and Model Comparisons

The two main results obtained so far are: 1. In isostatic computations linear approximation may result in significant distortions. Second and higher order approximations can be implemented very easily. 2. In addition to the classical Airy/Heiskanen local compensation model with constant compensation depth D, three models with degree dependent compensation depths D_n and a Vening-Meinesz regional compensation model have been derived.

We now turn to a comparison of the different models. In Figure 4 we show the spectra of the OSU81 (Rapp, 1981) field, the model with degree dependent D values based on criterion 3 and the Vening-Meinesz model with smoothing coefficients $\beta_n = e^{-b^2n^2}$ (D = 29 km, b = 0.00223). The D=30 km model, if plotted, would be almost the same as the Vening-Meinesz model. All models, except the one based on criterion 1, have less power than the observed

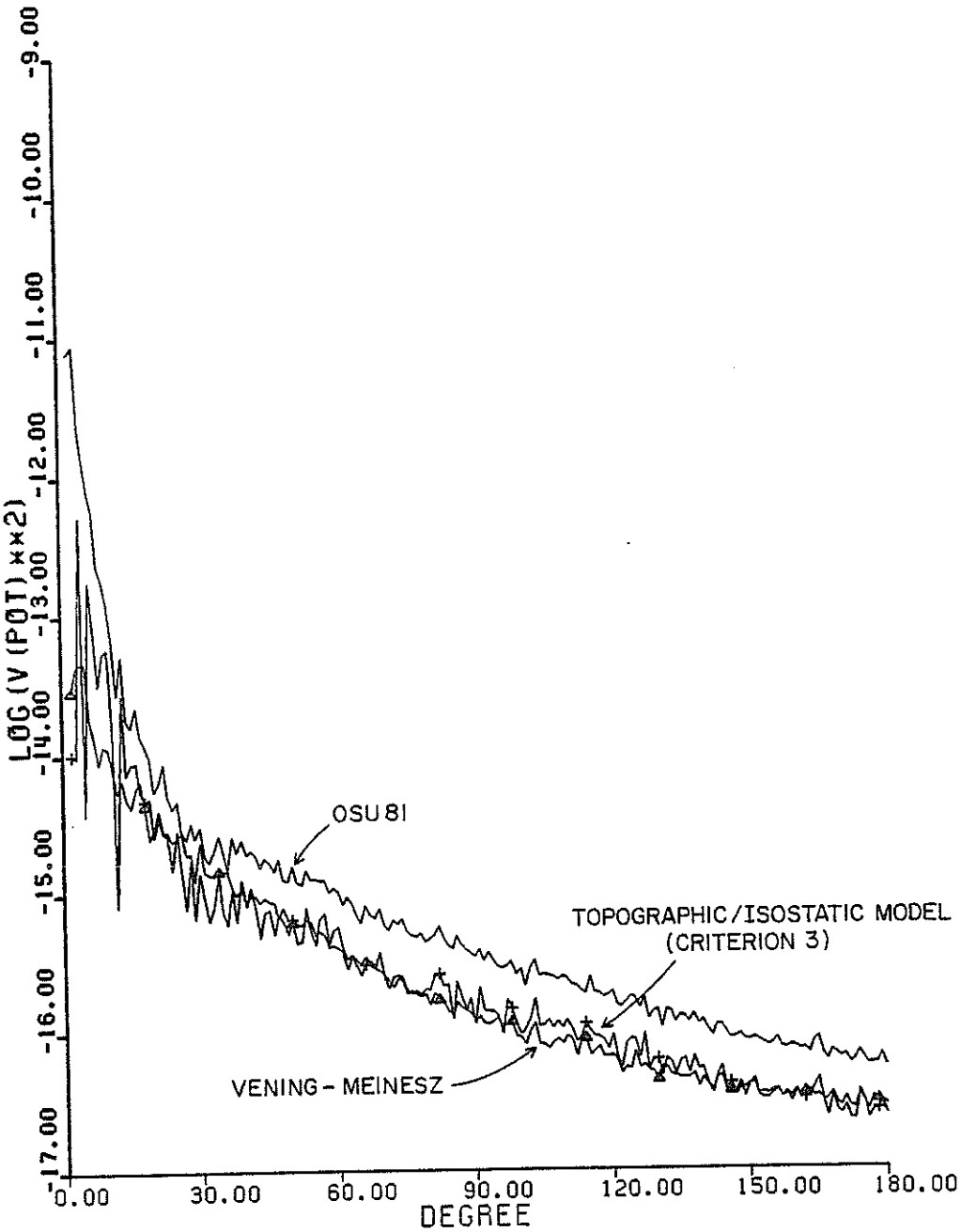

Figure 4. Log of the Potential Degree Variances of the OSU81 Potential Coefficient Solution, the Potential Implied by the Topographic/Isostatic Model Using Criterion 3, and the Potential Implied by the Vening-Meinesz Model, as a Function of Spherical Harmonic Degree.

potential at the higher degrees.

Next a set of quantities is introduced that can be used to compare two sets of potential coefficients. We define the difference between the coefficients $C_{nm\alpha}$ of the observed gravity potential and the isostatic coefficients $C^I_{nm\alpha}$ (model) as derived from the mean elevations by applying one of the five models as

$$\Delta C_{nm\alpha} = C_{nm\alpha} - C^I_{nm\alpha}\ (\text{model}). \tag{49}$$

The first quantity of interest is the root mean square undulation differences between degrees n_1 and n_2:

$$\delta N = \left[R^2 \sum_{n=n_1}^{n_2} \sum_m \sum_\alpha \Delta C^2_{nm\alpha}\right]^{1/2} \tag{50}$$

The next is the root mean square anomaly difference between degrees n_1 and n_2:

$$\delta g = \left[\gamma^2 \sum_{n=n_1}^{n_2} (n-1)^2 \sum_m \sum_\alpha \Delta C^2_{nm\alpha}\right]^{1/2} \tag{51}$$

We next have the percentage difference by degree:

$$P_n = \left[\frac{\sum_m \sum_\alpha \Delta C^2_{nm\alpha}}{\sigma^2_n(V)}\right]^{1/2} 100 \tag{52}$$

The average percentage difference between degree n_1 and n_2 is:

$$P = \frac{1}{n_2-n_1+1} \sum_{n=n_1}^{n_2} P_n \tag{53}$$

The $\sigma^2_n(V)$ are the dimensionless signal variances of the observed gravity potential as derived from the OSU81 set of spherical harmonic coefficients. As can be seen from the above formulas at each degree the relative behavior among the $\Delta C_{nm\alpha}$ derived from the five models remains the same in eqs. (50), (51), and (52). Only when the root mean square (r.m.s.) quantities in a range from degree n_1 to n_2 are computed this relative behavior could change. This is due to the multiplication by $(n-1)^2$ in (51) or the division by $\sigma^2_n(V)$ in (52), which changes the relative weight of certain degrees or degree ranges, respectively.

The root mean square undulation and anomaly differences are chosen, because they provide a good insight into the expected size of the residual undulation and anomaly field. The percentage difference is a valuable measure if the differences are small as compared to $\sigma^2_n(V)$. Its disadvantage is that it is unbounded, i.e. the percentage can reach infinity.

A parameter containing the same information as the percentage difference is the smoothing coefficient s_n. It has been used by Tscherning (1985) in comparing different geopotential models to the potential implied by the topography. It is defined as

$$s_n = \frac{\sum_m \sum_\alpha \Delta C^2_{nm\alpha}}{\sigma_n^2(V)} \tag{54}$$

Another measure is the correlation (coherence) coefficient by degree between $C_{nm\alpha}$ and $C^I_{nm\alpha}$ (model)

$$\rho_n = \frac{\sum_m \sum_\alpha C_{nm\alpha}\, C^I_{nm\alpha}(\text{model})}{\sigma_n(V)\sigma_n(V^I(\text{model}))} \tag{55}$$

Finally we have the average correlation coefficient between degree n_1 and n_2

$$\rho = \frac{1}{n_2 - n_1 + 1} \sum_{n=n_1}^{n_2} \rho_n \tag{56}$$

The degree correlation coefficient (or coherence coefficient) is a quantity that can be used to judge the agreement between any two quantities represented in a spherical harmonic expansion. Our particular case can be explained by taking the linear approximations to $C^I_{nm\alpha}$ from equation (24):

$$C^I_{nm\alpha} = \frac{3}{2n+1} \frac{\rho_{cr}}{\rho} \left[1 - \left(\frac{R-D}{R}\right)^n\right] h_{nm\alpha}$$

so that

$$\sigma_n(V^I) = \frac{3}{2n+1} \frac{\rho_{cr}}{\rho} \left[1 - \left(\frac{R-D}{R}\right)^n\right] \sigma_n(h)$$

Hence, in linear approximation the correlation coefficient per degree becomes, with (54):

$$\rho_n = \frac{\sum_m \sum_\alpha C_{nm\alpha} C^I_{nm\alpha}(\text{model})}{\sigma_n(V)\sigma_n(V^I(\text{model}))} = \frac{\sum_{m\alpha} C_{nm\alpha} h_{nm\alpha}}{\sigma_n(V)\sigma_n(h)} \tag{57}$$

The latter is the correlation coefficient between the observed gravity potential and the observed equivalent rock topography. We conclude that in linear approximation, the ρ_n are independent of the choice of the isostatic model. Consequently the differences in the correlation coefficients of the five models must be small and represent the influence of the second and higher order terms. In addition, since the second order term of $C^I_{nm\alpha}$ (cf. (24)) is positive by definition, one can show that the correlation coefficients of the linear models must be higher than those for the corresponding quantities in higher order approximations. On the other hand, since we know that the models in linear approximation represent rather unrealistic double layer models, we conclude that higher correlation coefficients do not necessarily imply a more realistic model.

Table 3 shows the anomaly, undulation and percentage differences, and the correlation coefficients for the various topographical isostatic models. The simple Airy model is represented through a D = 30 km depth of compensation. Other depths (28 and 32 km) were used but no significant changes noted. In addition, three degree ranges (2 to 180, 15 to 180, 30 to 180) have been used for the comparisons. All models yield very similar comparisons except for the case when D is computed by Criterion 1. This points out the clear problem of seeking D values that yield the same power as in the observed field.

Table 3. Comparisons Between OSU81 Model and Various Topographic/Isostatic Models for Three Different Degree Ranges.

Solution	Anomaly Diff (mgals)			Undulation Diff (meters)			Percentage Difference			Correlation Coefficient		
	2 180	15 180	30 180	2 180	15 180	30 180	2 180	15 180	30 180	2 180	15 180	30 180
D=30	20.64	16.27	15.43	30.57	2.30	1.46	81.48	80.51	80.41	.575	.599	.599
D=Crt1	24.11	17.64	16.74	45.35	2.48	1.58	89.19	87.18	87.18	.593	.616	.617
D=Crt2	20.16	16.27	15.42	29.59	2.31	1.47	80.48	80.54	80.38	.584	.603	.602
D=Crt3	20.15	16.12	15.30	29.59	2.26	1.44	80.43	79.75	79.75	.587	.603	.603
Vening-Meinesz	20.58	16.20	15.36	30.57	2.29	1.46	81.12	80.12	80.00	.581	.604	.605

Computations were also made with the TUG87 (Wiser, 1987) elevation model for selected cases. We found that this model yields better agreement with the OSU81 field than the TUG86 model. For example, using TUG87 the average percentage difference for D=30 km, degree 15 to 180, is 79.47% compared to 80.51% with TUG86. The correlation coefficient, in the same case is 0.614 as compared to 0.599. All computations were not carried out with TUG87 as it became available after most of the computations were completed for this paper.

Table 4 contains information on the smoothness coefficient (s_n) for selected degrees and for the same three degree ranges used previously. The smaller the s_n value, the better the agreement between the observed field and the models. All isostatic models, except that based on criterion 1, yield basically the same smoothing coefficients with those from criteria 2 and 3 being slightly better, i.e. smaller, for the 2 to 180 degree range. It lies in the very definition of criterion 3 - minimum norm of $dV = V - V^I$ - that the smallest values of $\Delta C_{nm\alpha}$ for each degree and therefore also of δN, δg, P_n, and s_n must be obtained with this criterion. In practice the differences between criteria 2 and 3 and the Vening-Meinesz model are very small. Obviously the smallest covariance values $cov_n(V^T, dV)$ must be obtained for criterion 2. We note that the use of the TUG87 model would have yielded slightly smaller P_n values. For example, for degree range 30 to 180, the s value is 0.626 for TUG87 vs 0.647 for TUG86.

Correlation coefficient information by degree range has been shown in Table 3. The correlation coefficients by degree show no significant variation between the models as expected. At degree 12 the correlation is about 0.04 which is unusual because most correlations in this degree area are on the order of 0.6. This small correlation at degree 12 also holds for other potential coefficient models.

Anomaly degree variances are a measure of the spectrum in the anomaly domain. We write:

Table 4. Relative Mean Square Coefficient Differences (s) Between OSU81 and Various Topographic/Isostatic Models

	Fixed D (km)	Variable D			Vening
ℓ	30	1	2	3	Meinesz
2	1.05	2.86	.98	.98	1.06
5	1.18	2.78	.97	.97	1.18
10	.68	.63	.53	.53	.68
12	1.18	1.89	1.05	1.05	1.16
15	.55	.58	.50	.50	.55
20	.76	.86	.75	.75	.75
25	.46	.51	.46	.46	.46
30	.73	.79	.67	.67	.72
50	.64	.78	.64	.64	.64
70	.59	.73	.59	.59	.59
90	.70	.90	.70	.70	.70
110	.60	.67	.58	.58	.58
130	.65	.76	.63	.63	.64
150	.68	.79	.68	.68	.67
170	.79	.95	.79	.79	.78
180	.67	.79	.67	.66	.66
2→180	.664	.796	.648	.647	.658
15→180	.648	.760	.649	.636	.642
30→180	.647	.760	.646	.636	.640

$$c_n = \gamma^2(n-1)^2 \sum_m \sum_\alpha C^2_{nm\alpha} \tag{58}$$

The c_n values computed from the models used in this paper are interpreted to refer to a sphere corresponding to the mean earth radius of 6371 km due to the spherical approximations of the model. Values of c_n are given in Table 5. The model with the most power is the variable D case with criterion 1. The other models have power by degree, and cumulatively, that is significantly less than what is in the observed field as represented by the OSU81 field.

The coefficients have next been used to create gravity anomaly maps in the Carribean region and in northern South America. This area was selected due to the complex nature of the gravity field due to the presence of both a trench area (the Puerto Rican Trench) and a substantial mountain range (the Andes Mountains). From the point of view of an area where isostatic compensation would be most apparent, this area may not be ideal. These maps have been created using the potential coefficients from degree 30 to 180 of the OSU81 field (Figure 5) and the Vening-Meinesz regional compensation field (Figure 6). The anomaly plots for the D=30 km case and the depths from criterion 1 case are very similar.

The OSU81 field reflects the known anomaly field structure in this region. There is clearly a correlation of the significant anomaly structure between the

OSU81 field and the topographic/isostatic model. However the range of the anomalies is much smaller in the model case.

Table 5. Anomaly Degree Variances (mgal^2)

		Fixed D	Variable D			Vening-Meinesz
ℓ	OSU81	30 km	1	2	3	
15	3.0	0.9	3.0	1.1	1.6	0.8
30	2.5	2.0	2.4	1.1	1.1	1.9
50	3.6	1.4	3.6	1.4	1.5	1.4
70	2.7	1.1	2.6	1.1	1.1	1.2
90	2.6	0.9	2.6	0.8	0.9	0.9
100	2.6	0.8	2.6	0.9	0.9	0.8
120	2.1	0.8	2.6	1.1	1.3	0.9
140	2.2	0.8	2.2	1.0	1.0	0.8
160	1.8	0.8	1.8	0.8	0.9	0.9
180	1.6	0.8	1.5	0.7	0.7	0.9
2→180	586	176	582	201	210	181
15→180	412	169	408	173	182	174
30→180	372	149	368	155	164	155

Quantities that are primarily used in the geophysical literature are the continental and oceanic response functions. The response function (as discussed here) is a measure of the transfer of information between topography and gravity field quantities, such as Bouguer or free air gravity anomalies. Discussions of response functions in flat earth approximation applying two dimensional Fourier transforms can be found, for example in (Dorman & Lewis, 1970; McKenzie & Bowin, 1976, or McNutt, 1979). A general review is given by Boekelo (1985). A discussion of the response function technique for a spherical earth can be found in (Dorman & Lewis, ibid), (Boekelo, ibid), (Cazenave et al., 1986) and other sources.

The response function technique assumes a linear relationship between gravity anomalies and equivalent rock topography. Let us define the coefficients of the free air gravity anomaly field as

$$g^f_{nm\alpha} = \gamma(n-1)C_{nm\alpha} \tag{59}$$

and those of the Bouguer gravity anomaly field (compare (25a)) as

$$g^b_{nm\alpha} = \gamma(n-1)\ \{C_{nm\alpha} - C^T_{nm\alpha}\}$$

$$= \gamma(n-1)\ \left\{C_{nm\alpha} - \frac{3}{2n+1}\,\frac{\rho_{cr}}{\bar{\rho}}\,h_{nm\alpha}\right\} \tag{60}$$

Then the assumption is that there exists an unknown linear transfer function $Z_n\ (g^f,h)$ such that

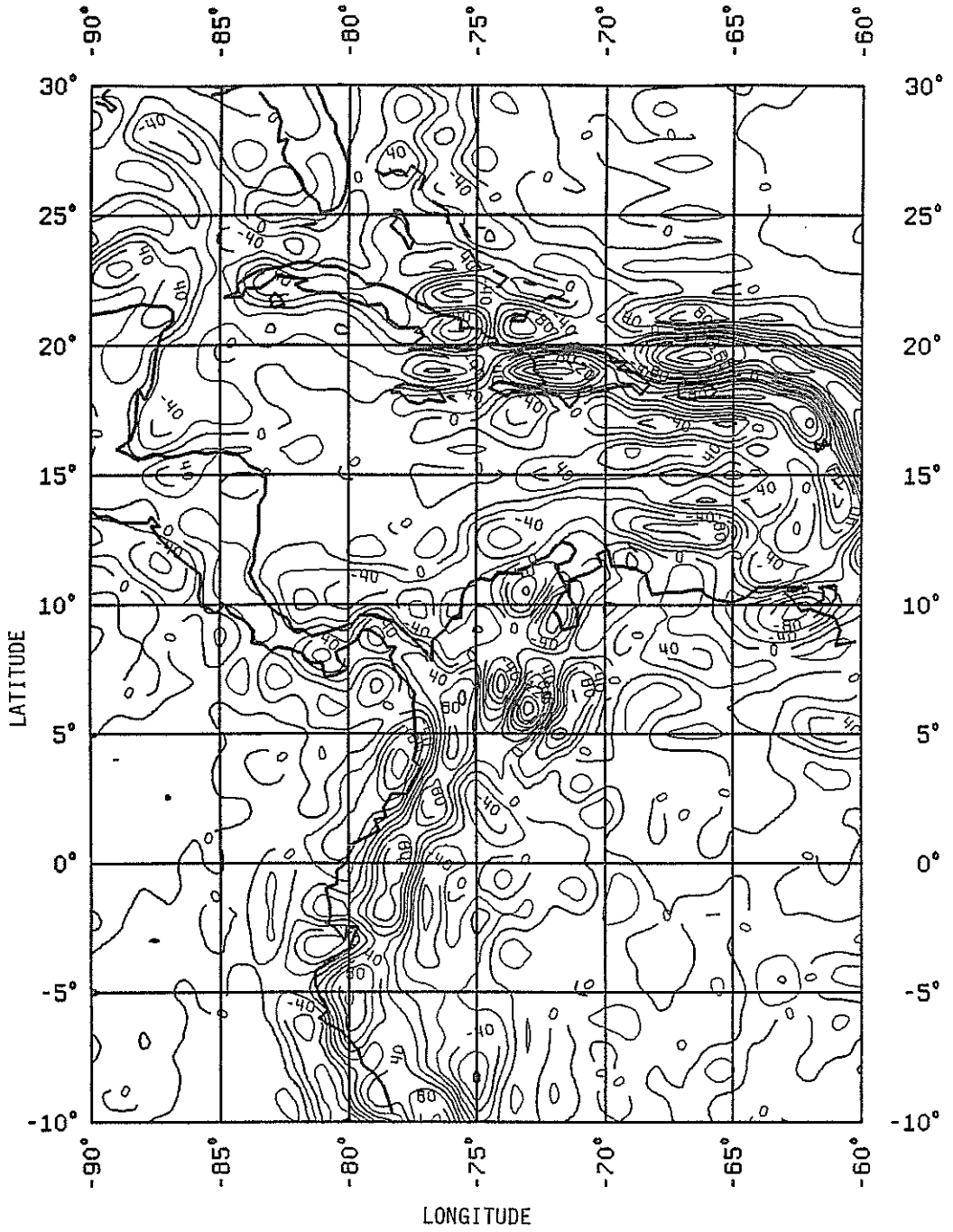

Figure 5. Free-Air Gravity Anomalies Implied by the OSU81 Field from Degree 30 to Degree 180 in Northern South America and the Caribbean; Contour Interval = 20 mgal.

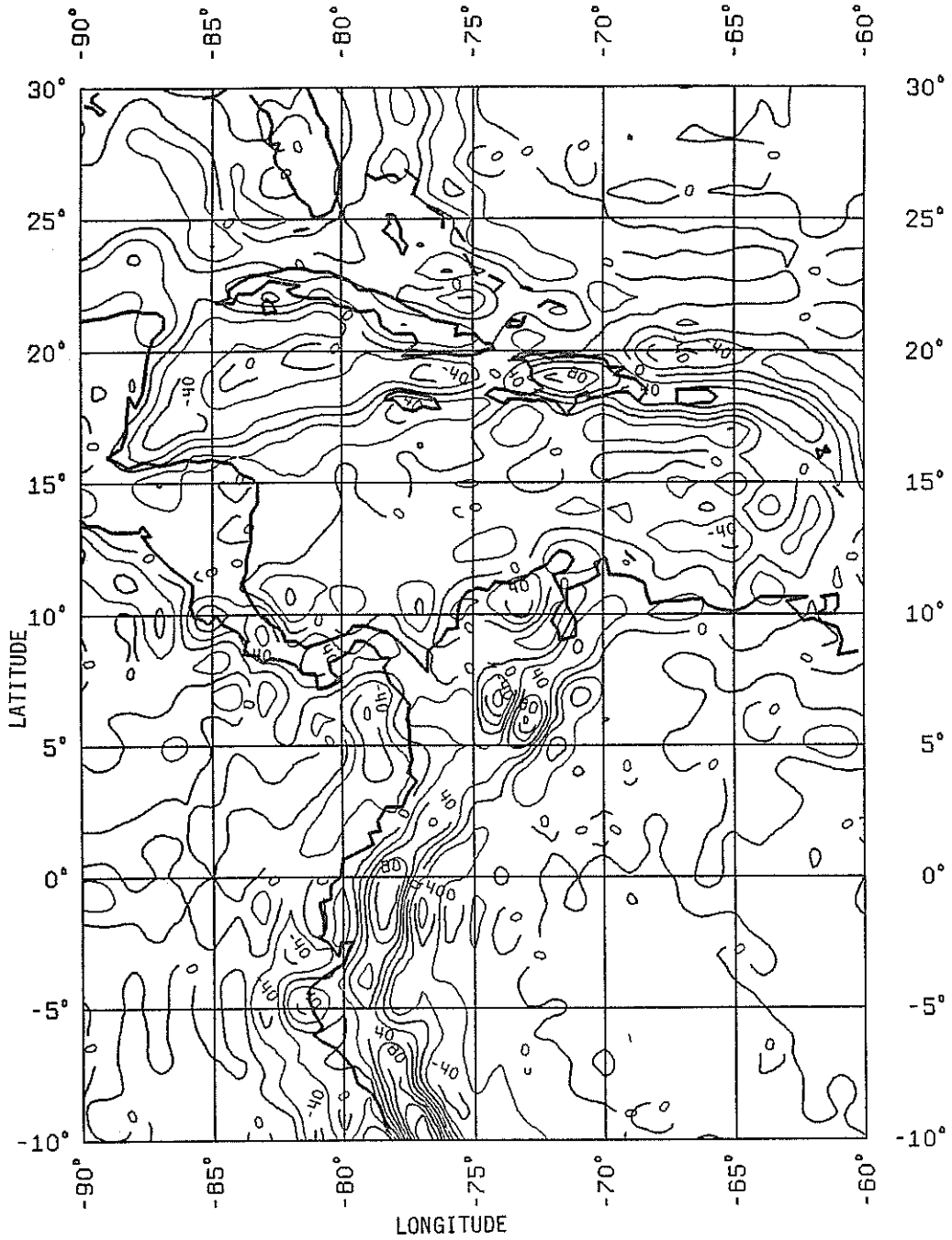

Figure 6. Free-Air Gravity Anomalies Implied by the Vening-Meinesz Model from Degree 30 to Degree 180 in Northern South America and the Caribbean Sea; Contour Interval = 20 mgal.

$$g^f_{nm\alpha} = Z_n\ (g^f, h)\ h_{nm\alpha} + e^f_{nm\alpha} \tag{61}$$

and a transfer function $Q_n\ (g^b, h)$ such that

$$g^b_{nm\alpha} = Q_n(g^b,\ h)h_{nm\alpha} + e^b_{nm\alpha} \tag{62}$$

In both cases the $e^f_{nm\alpha}$ and $e^b_{nm\alpha}$ are assumed to be small and (almost) randomly distributed. Then the coefficients Z_n and Q_n can be determined in the least-squares sense from

$$Z_n(g^f,\ h) = \frac{\sum_m \sum_\alpha g^f_{nm\alpha}h_{nm\alpha}}{\sum_m \sum_\alpha h_{nm\alpha}h_{nm\alpha}} \tag{63}$$

and

$$Q_n(g^b,\ h) = \frac{\sum_m \sum_\alpha g^b_{nm\alpha}h_{nm\alpha}}{\sum_m \sum_\alpha h_{nm\alpha}h_{nm\alpha}} \tag{64}$$

In function Z_n is usually referred to as <u>oceanic or free-air response</u>, whereas Q_n is denoted isostatic or <u>continental or Bouguer response</u>.

The theoretical values of Z_n and Q_n for our five models become

$$Z_n = \gamma(n-1)\ \frac{3}{2n+1}\ \frac{\rho_{cr}}{\bar{\rho}}\ \left[1 - \left[\frac{R-D}{R}\right]^n \beta_n\right] \tag{65}$$

and

$$Q_n = \gamma(n-1)\ \frac{3}{2n+1}\ \frac{\rho_{cr}}{\bar{\rho}}\ \left[\frac{R-D}{R}\right]^n \beta_n \tag{66}$$

where

$\beta_n = 1$ for the Airy/Heiskanen model (D = const)

$\beta_n = \left[\frac{R-D_n}{R-D}\right]^n$ for the models based on criteria 1, 2, and 3 and

$\beta_n = e^{-b^2n^2}$ for the Vening Meinesz model.

Figure 7 shows the oceanic (free-air) response functions Z_n of our five models and as directly derived from the data. It can be seen that they all agree very well, except the one based on criterion 1. As to be expected, the free air anomaly field has little correlation with the topography at low frequencies whereas for high frequencies the correlation increases. It is remarkable that the response as derived from the data stays significantly below that determined from the models for wavelengths smaller than 300 km.

In Figure 8 the analogous curves of the continental (Bouguer) response functions are given. Again the curve based on criterion 1 departs from all others. For the long wavelengths down to 2000 km all other curves show approximately a Q_n value of -0.10 mgal/m, somewhat lower than the well known Bouguer gradient of -0.1119 mgal/m. For small wavelength the correlation of the Bouguer anomalies with topography decreases, as to be expected.

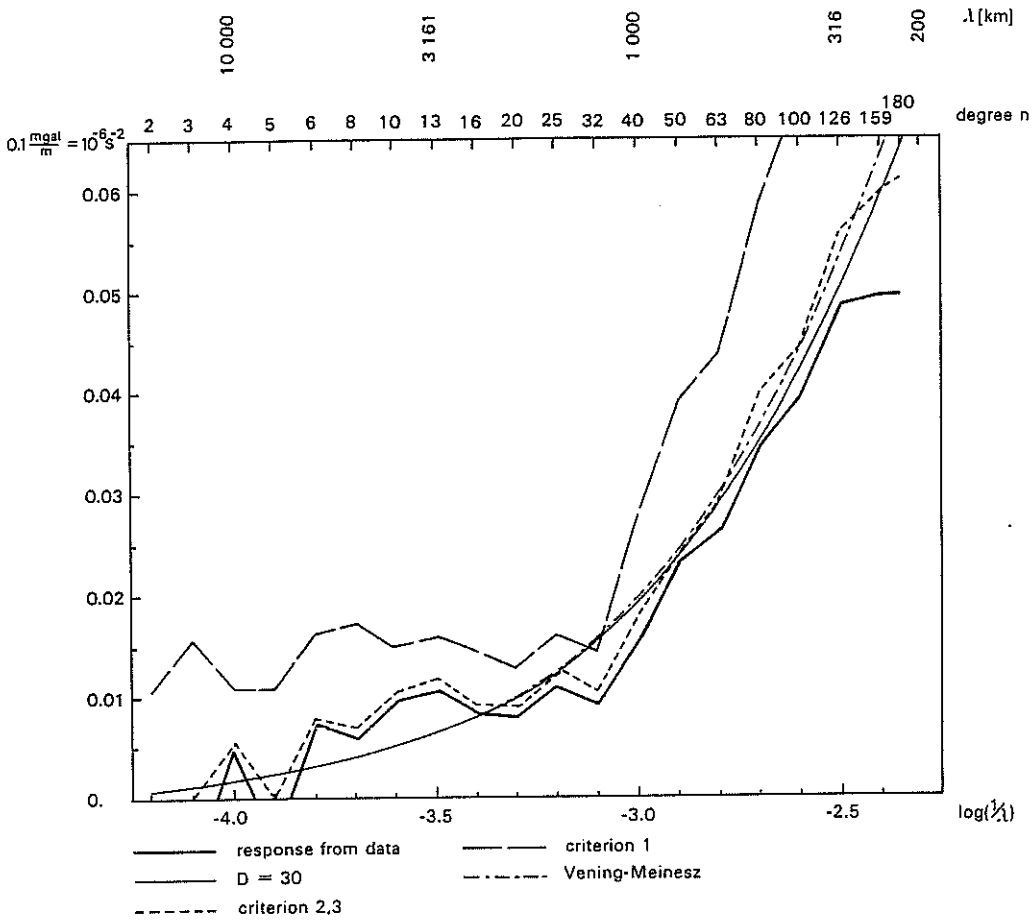

Figure 7. The Oceanic (Free-Air) Response Function, Z_n (in 0.1 mgal/m) By Degree, for Various Topographic/Isostatic Models, and as Derived From the OSU81 Model.

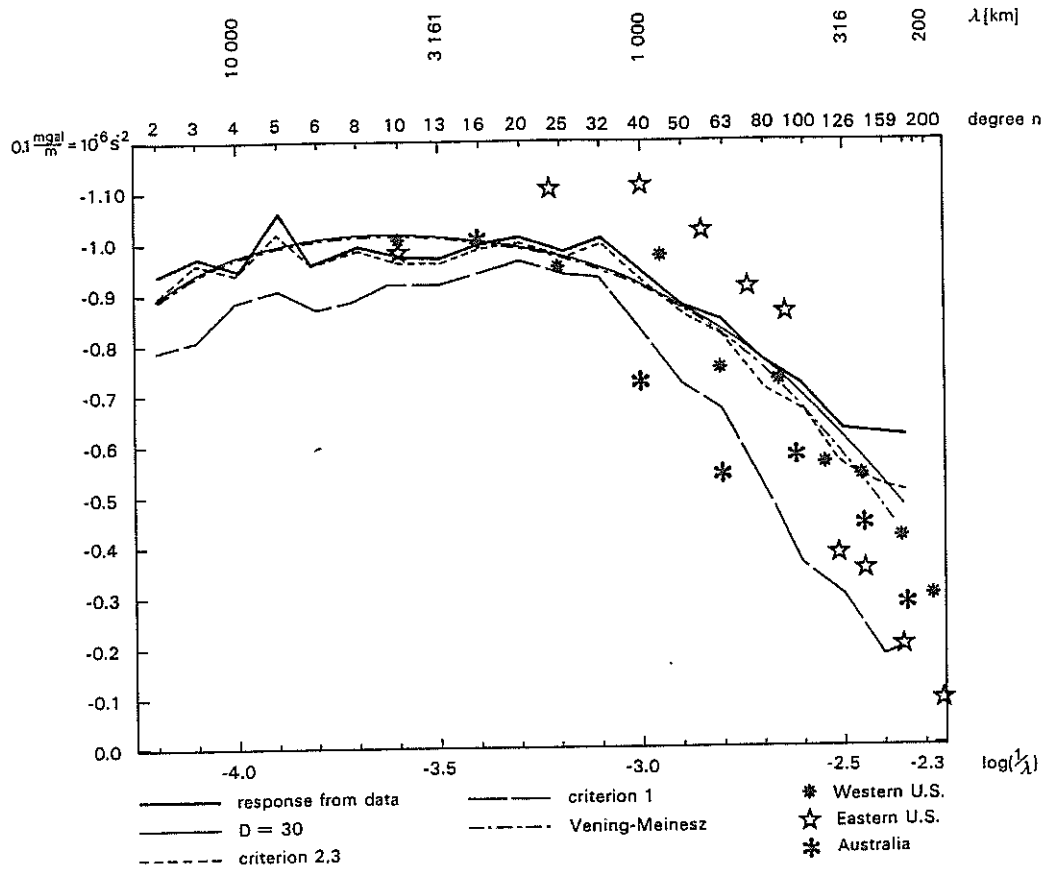

Figure 8. The Continental (Bouguer) Response Function Q_n (in 0.1 mgal/m), by Degree, for Various Topographic/Isostatic Models and as Derived From the OSU81 Model, with Sample Values From Regional Studies.

Also shown on Figure 8 are sample values of continental response of Eastern U.S., Western U.S., and Australia, as derived from regional studies. The values are taken from (McNutt, 1978 and 1980). The values are scattered around the curves of the global models and data. This would indicate that our data can be seen as a global average. Only for wavelengths smaller than about 400 km are the sample values throughout smaller, which could indicate that especially for these wavelengths there exists a significant difference in response between continental and oceanic lithosphere. It should be pointed out again, that a general drawback of the response technique is, that it assumes a linear relationship and consequently implies a simple, double layer approximation.

9. Conclusions

This paper has considered improved procedures to compute the topographic/isostatic effects due to Airy compensation taking into account three terms in a series expansion. Normally only the first term is used. Tests showed that the second term in an expansion contributes an average of 30% of the first term while the third term contributes an average of 3%. Overall differences between one and three component models of ±4.4 mgal and 35% indicate the importance of the higher order terms. The potential field implied by this theory has been compared with an observed field defined by a set of potential coefficients to degree 180. Comparisons were also made with a Vening-Meinesz type model derived by Sünkel. Comparisons were carried out for fixed depths of compensation and for depths computed as a function of spherical harmonic degree using three different criteria. Two of these criteria (II and III) led to nearly the same depths of compensation while criterion I led to depths of compensation larger than normally accepted for the Airy hypothesis. The results of the comparison of the theoretical models with the observed field were given in Tables 3, 4, 5. No substantial differences occur between the models except for the case of depth Criterion I which implies substantially poorer agreement with the observed field.

The rather high compensation depths D_n, for the very low degrees, that were obtained, when applying criteria 1, 2, and 3 (see Table 2) could be an indication that the compensation of the large scale topographic features cannot be explained by some simple Airy or Vening-Meinesz type of model. The great depths could be a hint that the long wavelengths compensation is related to the convection mechanism in the upper mantle.

The Vening-Meinesz model applied by Sünkel results in the response function (cf. (54) and (65)):

$$Q_n = \gamma(n-1)\,\frac{3}{2n+1}\,\frac{\rho_{cr}}{\Delta\rho}\left[\frac{R-D}{R}\right]^n \beta_n \qquad (67)$$

with $\beta_n = e^{-b^2 n^2}$. Turcotte & Schubert (1982) discuss the flexure of the lithosphere under periodic loading, derived from the equation of equilibrium of a deformed plate. The result - when transformed from a plane to a spherical approximation - is a smoothing factor

$$\beta_n = \left[1 + \frac{D'}{\gamma \Delta\rho} \left(\frac{n}{R}\right)^4\right]^{-1}$$

where D' is the flexural rigidity (see also e.g. (Banks et al., 1977)). Hence this smoothing model behaves basically as $1/(1+kn^4)$ with k a constant. It can easily be shown that a smoothing model with $e^{-b^4 n^4}$ and an appropriate choice of b, can be made to agree almost perfectly with the above expression. This allows us to interpret the constant b of the Vening-Meinesz regional compensation model in terms of the flexural rigidity D' of the the deformed plate model in (Turcotte & Schubert, ibid).

Four of the five models discussed here show a very similar overall behavior, despite the different assumptions on which they are based. This leads to a twofold conclusion. First, a rather large variation in the chosen isostatic models has little effect on the resulting isostatic gravity potential. Second, the other way round, despite today's availability of rather good observed gravity and topographic elevations, the data are not selective enough to identify one particular isostatic model. This also implies that the uncertainty of parameters derived from the isostatic models, when dealing with global models. It means also that one of the two primary objectives, stated in the introduction can hardly be met, namely to isolate and display those parts in the anomalous gravity field, that are not compensated isostatically, but are due to lateral inhomogeneities in the earth's mantle. This basically reconfirms Dahlen (1982; p. 3947) who states "... that this can never be done unequivocally even if the topography d and density anomalies ρ_1 are known exactly, since it requires that the concept of local isostasy be defined extremely precisely, more precisely, in fact, then the concept itself probably warrants."

The remaining gravity potential, after subtracting the isostatic part from the observed one, must to some extent be attributed to the fact, that the approach chosen here does not easily allow the application of different isostatic models for different tectonic zones (e.g. continents and ocean areas) and that no corrections were made for geoid-age, depth-age effects or sediment loading as has been done e.g. in (Cazenave et al., 1986) or (McNutt and Shure, 1986).

Since the isostatic behavior of the earth is dependent on a number of factors, and considering that such behavior varies substantially from area to area, global models cannot be expected to reflect the full picture. This paper, however, has examined what can be learned from global modeling techniques, and does not imply that the mechanisms employed are the only ones involved in the complex physical process of isostasy.

Our results and conclusions depend to a lesser extent on the accuracy of the topographic model and the observed potential field model. The topographic model used is a clear improvement over previous models. However we still do not have ice thickness used in the computations. The observed potential field could be updated to more current models (e.g. Rapp and Cruz, 1986, Wenzel, 1985) but no substantial changes are expected.

References

Arnold, K., The Isostatic Potential Including Second Order Terms, Gerlands Beitr. Geophysik. Leipzig 89, 289-293, 1980.

Balmino, G., K. Lambeck, and W. Kaula, A spherical Harmonic Analysis of the Earth's Topography, J. Geophy. Res., Vol. 78, No. 2, 478-521, 1973.

Banks, R.J., R.L. Parker, and J.P. Huestis, Isostatic compensation on a local scale: Local versus regional mechanisms, Geophys. J. Roy. Astron. Soc., 51, 431-452, 1977.

Boekelo, G., Modern Isostasy, Technische Hogeschool, Afdeling der Geodesie, Delft, 1985.

Cazenave, A., K. Dominh, C. Allegre, and J. Marsh, Global Relationship Between Oceanic Geoid and Topography, J. Geophys. Res., 91, 11,439 - 11,450, 1986.

Colombo, O., Numerical Methods for Harmonic Analysis on the Sphere, Report No. 310, Dept. of Geodetic Science, The Ohio State University, Columbus, 1981.

Dahlen, F., Isostatic Geoid Anomalies on a Sphere, J. Geophys. Res., 87, 3943-3948, 1982.

Dorman, L.M. and B.T.-R. Lewis, Experimental Isostasy: 1, Theory of the Determination of the Earth's Isostatic Response to a Concentrated Load, J. Geophys. Res., 75, 17, 3357 - 3365, 1970.

Forsberg, R. and C.C. Tscherning, The Use of Height Data in Gravity Field Approximation by Collocation, J. Geophys. Res. 86, B9, 7843-7854, 1981.

Jung, K., Die Rechnerische Behandlung der AIRYschen Isostasie mit einer Entwicklung des Quadrats der Meereshoehen nach Kugelfunktionen. Sonderdruck aus Gerlands Beiträge zur Geophysik, 62, Helff 1, 39-56, 1950.

Lachapelle, G., A Spherical Harmonic Expansion of the Isostatic Reduction Potential, Bull. Geod. e Sci. Aff. 35, 281-299, 1976.

McKenzie, D.P., and C. Bowin, The Relationship Between Bathymetry and Gravity in the Atlantic Ocean, J. Geophys. Res., 81, 1903 - 1915, 1976.

McNutt, M., Compensation of Oceanic Topography: An Application of the Response Function Technique to the Surveyor Area, J. Geophys. Res., 84, 7589-7597, 1979.

McNutt, M., Implications of regional gravity for state of stress in the Earth's crust and upper mantle, J. Geophys. Res., 85, 6377-6396, 1980.

McNutt, M., and L. Shure, Estimating the Compensation Depth of the Hawaiian Swell With Linear Filters, J. Geophys. Res., 91, 13,915 - 13,923, 1986.

NGDC, Global Gridded Bathymetric Data, SYNBAPS II, National Geophysical Data Center announcement 83-MGa-11, 1983

Rapp, R.H., The Earth's Gravity Field to Degree and Order 180 Using Seasat Altimeter Data, Terrestrial Gravity Data, and Other Data, Report No. 322, Dept. of Geodetic Science, The Ohio State University, Columbus, 1981.

Rapp, R.H., Degree Variances of the Earth's Potential, Topography and its Isostatic Compensation, Bulletin Géodésique, 56, 84-94, 1982.

Rapp R.H., and J.Y. Cruz, The Representation of the Earth's Gravitational Potential In A Spherical Harmonic Expansion to Degree 250, Report No. 312, Dept. of Geodetic Science and Surveying, The Ohio State University, Columbus, 1986.

Sünkel, H., An Isostatic Earth Model, Report No. 367, Dept. of Geodetic Science and Surveying, The Ohio State University, Columbus, 1985.

Sünkel H., Global Topographic - Isostatic Models, in Mathematical and Numerical Techniques in Physical Geodesy, Lecture Notes in Earth Sciences, Springer-Verlag, Berlin, 1986.

Tscherning, C.C., On the Long-Wavelength Correlation Between Gravity and Topography, in proc. of the 5th Int. Symp. "Geodesy and Physics of the Earth", published by Central Institute for Physics of the Earth, Potsdam, DDR, 1985.

Turcotte, D. and G. Schubert, Geodynamics applications of continuum physics to geological problems, Wiley, 450 pp., New York, 1982.

Uotila, U.A., Prediction of Gravity Anomalies Using a Mathematical Model, Report No. 59, Dept. of Geodetic Science, The Ohio State University, Columbus, 1965.

Vening Meinesz, F.A., Tables Fundamentales Pour la Réduction Isostatique Régionale, Bulletin Geodesique, No. 63, 771 - 776, 1939.

Wenzel, H-G., Hochauflösende Kugelfunktions modelle für das Gravitations - potential der Erde, Wiss. Arb. Fachrichtung Vermessungswesen der Universitaet Hannover, 1985.

Wiser, M., The Global Digital Terrain Model TUG87, internal report, Technical University Graz, Institute of Mathematical Geodesy, 1987.